Kaon and pion femtoscopy at the highest energies available at the BNL Relativistic Heavy Ion Collider (RHIC) in a hydrokinetic model

Iu. A. Karpenko and Yu. M. Sinyukov
Bogolyubov Institute for Theoretical Physics, Metrolohichna Strasse 14b, 03680 Kiev, Ukraine
(Received 9 April 2010; published 13 May 2010)

The hydrokinetic approach that incorporates hydrodynamic expansion of the systems formed in $A + A$ collisions and their dynamical decoupling is applied to restore the initial conditions and space-time picture of the matter evolution in central Au + Au collisions at the top Relativistic Heavy Ion Collider energy. The analysis is based on the detailed reproduction of the pion and kaon momentum spectra and femtoscopic data in whole interval of the transverse momenta studied by both the STAR and the PHENIX collaborations. The fitting procedure utilizes the two parameters: the maximal energy density at supposed thermalization time 1 fm/c and the strength of the prethermal flows developed to this time. The quark-gluon plasma and hadronic gas is supposed to be in complete local equilibrium above the chemical freeze-out temperature $T_{\rm ch} = 165$ MeV with the equation of states (EoS) at high temperatures as in the lattice QCD. Below $T_{\rm ch}$ the EoS in the expanding and gradually decoupling fluid depends on the composition of the hadron-resonance gas at each space-time point and accounts for decays of resonances into the nonequilibrated medium. A good description of the pion and kaon transverse momentum spectra and interferometry radii is reached at both used initial energy density profiles motivated by the Glauber and color glass condensate models, however, at different initial energy densities. The discussion as for the approximate pion and kaon m_T scaling for the interferometry radii is based on a comparison of the emission functions for these particles.

DOI: 10.1103/PhysRevC.81.054903 PACS number(s): 25.75.Cj, 25.75.Ld

I. INTRODUCTION

At present the majority of the dynamical models of $A + A$ collisions which describe the soft-physics phenomena are based on the Landau's idea [1] of space-time evolution of the thermal matter formed in the collisions. This approach implies at once the specific space-time scales in the problem of nuclear scattering such as a time of expansion, a volume occupied by the fireball, hydrodynamic lengths, etc. The only direct tool for measuring at these femtoscopic scales is the intensity interferometry method, now often called femtoscopy. The measured scales—the interferometry, or Hanbury Brown–Twiss (HBT) radii—are associated just with the homogeneity lengths in the rapidly expanding system created in heavy-ion collisions [2]. So comparing experimental data of the space-time scales characterizing such a dynamical model of the system evolution and particle production should be one of the first tasks in justifying the model and discriminating between different approaches. Nevertheless, such a comparison was often ignored because almost all dynamic models, which pretend to be complete and therefore describe the evolution of the matter as well as its gradual decay, for example, the hybrid [hydrodynamic plus ultrarelativistic quantum molecular dynamics (UrQMD)] models [3], failed to reproduce pion out-, side-, and long-interferometry radii simultaneously with the hadronic spectra at the Relativistic Heavy Ion Collider (RHIC). Until now it was possible to reach only when some artificial parametrization of freeze-out processes, for example, a sudden freeze-out at a fairly large temperature close to the hadronization one [4], is utilized.

In Refs. [5–7] the hydrokinetic model (HKM) for $A + A$ collisions has been developed. It combines the advantages of the hydrodynamic approximation, where possible phase transitions are encoded in the corresponding equation of state (EoS), and the microscopic approach, accounting for a nonequilibrated process of the spectra formation owing to gradual particle liberation. The dynamical decoupling is described by the particle-escape probabilities in inhomogeneous hydrodynamically expanding systems in a way consistent with the kinetic equations in the relaxation-time approximation for emission functions [5]. The method can be applied to match correctly hydrodynamics and UrQMD, using as the input the locally nonequilibrated distribution functions from the HKM. Then one can match these models at spacelike hypersurfaces related to the late stage of the evolution, escaping thus the inconsistencies connected with an inapplicability of hadron cascade models at very high densities and with the causality [8].

The HKM method also allows one to take into account a back reaction of particle emission on the hydrodynamic evolution that corresponds an account of the viscous effects at the hadronic stage of the evolution [6]. It is worth noting that the ratio of the shear viscosity to the total entropy obtained in HKM model is less than $1/2$ in the space-time region of maximal hadronic emission [9]. An analysis of the quark-gluon plasma (QGP) evolution within viscous hydrodynamics is also a topical problem because the shear viscosity brings an important effect, an increase of transverse flows during the evolution [10]. However, until the viscosity of the QGP as the function of the temperature becomes clear, this effect is simpler to take into account in the phenomenological way, as is proposed in what follows.

In this article we apply the HKM [5,6] to an analysis of the femtoscopic measurements at RHIC for central Au + Au collisions at the top energy $\sqrt{s} = 200$ A GeV. Namely, we

analyze pion and kaon transverse momentum spectra and the m_T behavior of the pion and kaon interferometry radii to clarify, in particular, how these observables depend on the initial conditions: Glauber- and color glass condensate (CGC)-like. The basic hydrokinetic code, proposed in Ref. [6], is modified now to include decays of resonances into the expanding hadronic chemically nonequilibrated system and, based on the resulting composition of the hadron-resonance gas at each space-time point, to calculate the EoS in the vicinity of this point. The obtained local EoS allows one to determine the further evolution of the considered fluid elements. In the zone of chemical equilibrium, above the chemical freeze-out temperature, the EoS is taken in accordance with the lattice QCD results.

The article is organized as Follows. Section II is devoted to the initial conditions (IC) for thermal evolution of the matter in Au + Au collisions at RHIC. In Sec. III we discuss the EoS of the matter in equilibrated and chemically nonequilibrated zones. The kinetics of the system in the nonequilibrium zone related to the system's evolution and decoupling is described in Sec. IV. The underlying hydrodynamic model for both chemically equilibrated and nonequilibrated domains is presented in Sec. V. Section VI is devoted to the results obtained and discussions. The conclusions and outlook are presented in Sec. VII.

II. INITIAL CONDITIONS FOR HYDROEVOLUTION OF THERMAL MATTER

Our results are all related to the central rapidity slice where we use the boost-invariant Bjorken-like initial condition in the longitudinal direction. We consider the proper time of thermalization of quark-gluon matter as the minimal one discussed in the literature, $\tau_0 = 1$ fm/c [11].

A. Prethermal flows

If one starts the hydrodynamic evolution at the "conventional time" $\tau_i = 1$ fm/c *without* transverse flow—because no pressure is established before thermalization—the resulting radial flow will not be developed enough to describe simultaneously the absolute values of pion, kaon, and proton spectra, as well as the anisotropy of elliptic flow in noncental collisions. To describe the observables, one needs to start the hydroevolution at very small initial time, $\tau \sim 0.5$ fm/c [12], where it is difficult to expect the thermalization. This controversial situation is overcome owing to the results of Ref. [13], where it is shown that the initial transverse flows in thermal matter, as well as their anisotropy leading to asymmetry of the transverse momentum spectra in noncentral collisions, could be developed at the prethermal, either classical field (Glasma) [14], string [15], or partonic stages, with even more efficiency than in the case of very early hydrodynamics. So, the hypotheses of early thermalization at times less than 1 fm/c is not necessary: The radial and elliptic flows develop regardless of whether a pressure is already established. The general reason for them is an essential finiteness of the system in the transverse direction. Then the flows of particle number or energy directed outward from the system cannot be compensated by the inward-directed (from periphery to the center) flows. This difference results in nonzero net flows no matter how the collective velocity is defined, according to Ekkart or to Landau-Lifshitz. Further development and exploitation of these results is presented in Refs. [16–18].

The initial transverse rapidity profile is supposed to be linear in radius r_T:

$$y_T = \alpha \frac{r_T}{R_T}, \quad \text{where} \quad R_T = \sqrt{\langle r_T^2 \rangle}, \tag{1}$$

where α is the second fitting parameter. Note that the fitting parameter α should include also a positive correction for underestimated resulting transverse flow because in this work we did not account in a direct way for the viscosity effects [10] at the QGP stage or the hadronic stage. In the formalism of HKM [6], the viscosity effects at the hadronic stage are incorporated in the mechanisms of the back reaction of particle emission on hydrodynamic evolution, which we ignore in current calculations. Because the corrections to transverse flows, which depend on unknown viscosity coefficients, are unknown, we use fitting parameter α to describe the "additional unknown portions" of flows caused by prethermal flow development and the viscosity effects in QGP.

B. Glauber-like initial transverse profile

A simple Glauber model initialization assumes that the initial energy density in the transverse plane is proportional to the participant nucleon density [19],

$$\epsilon(\mathbf{b}, \mathbf{x}_T) = \epsilon_0 \frac{\rho(\mathbf{b}, \mathbf{x}_T)}{\rho_0}, \tag{2}$$

with $\rho_0 \equiv \rho(0, 0)$ and

$$\begin{aligned} \rho(\mathbf{b}, \mathbf{x}_T) &= [T(\mathbf{x}_T + \mathbf{b}/2) S(\mathbf{x}_T - \mathbf{b}/2) \\ &\quad + T(\mathbf{x}_T - \mathbf{b}/2) S(\mathbf{x}_T + \mathbf{b}/2)], \\ S(\mathbf{x}_T) &= \left\{ 1 - \left[1 - \sigma_{NN} \frac{T(\mathbf{x}_T)}{A} \right]^A \right\}, \end{aligned} \tag{3}$$

where A is atomic number, equal to 197 for Au + Au collisions, and $\sigma_{NN} = 51$ mb (=5.1 fm^2) is the nucleon-nucleon cross section at $\sqrt{s_{NN}} = 200$ A GeV. The impact parameter $\mathbf{b} = (b, 0)$ is equal to zero, $b = 0$, in the considered case of central collision. The parameter $\epsilon_0 \equiv \epsilon(b = 0, \mathbf{x}_T = 0)$ is the maximal energy density at the initial moment of thermalization. The thickness $T(\mathbf{x}_T)$ is expressed through the Woods-Saxon distribution profile:

$$T(\mathbf{x}_T) = \int_{-\infty}^{\infty} F_{\mathrm{WS}}(\mathbf{x})\, dx_L, \tag{4}$$

where

$$F_{\mathrm{WS}}(\mathbf{x}) = \frac{a}{\exp\left[\left(\sqrt{x_L^2 + x_T^2} - R_A \right) / \delta \right] + 1}. \tag{5}$$

Here we use that $R_A = 1.12A^{1/3} – 0.86A^{-1/3} \approx 6.37$ fm, $\delta = 0.54$ fm. Constant a is obtained from the normalization condition:

$$\int T(\mathbf{x}_T)\, d^2 x_T = A. \tag{6}$$

One can think that transversal Glauber-like ϵ profile has been formed to some initial time $\tau_0 \approx 0.1$–0.3 fm/c (see later in this article) when the system is not thermal yet. However, the form of the profile is, practically, not modified to supposed thermalization time $\tau_0 \sim 1$ fm/c because the transverse velocities reached up to this time are relatively small. At the same time, the absolute values of energy density can change significantly because of the strong longitudinal expansion. We use the maximal energy density ϵ_0 at time $\tau_i = 1$ fm/c as the second fitting parameter.

C. Initial conditions motivated by the color glass condensate model

Within CGC effective field theory, some important physical properties of the field are defined by the parameter $\Lambda_s = g^2\mu$, where $g^2 = 4\pi\alpha_s$ and μ^2 is a dimensionless parameter, which is the variance of the Gaussian weight over the color charges ρ of partons. The value of Λ_{s0} is approximately equal to the saturation scale value, Q_s, and for the RHIC energies one can use $\Lambda_{s0} \approx Q_s \approx 2$ GeV^2 [20]. According to the results of Refs. [21,22], (proper) time $\tau_0 \approx 3/\Lambda_s$ is an appropriate scale controlling the formation of gluons with a physically well-defined energy. At later times the dynamics of the classical Yang-Mills fields produced in nucleus-nucleus collisions can be linearized and approximated by that of a system of weakly coupled harmonic oscillators. Then one can compute the field amplitudes squared in momentum space and find the corresponding distribution for the gluon number [22,23] for a cylindrically homogeneous transverse profile. It has the following form at $p_T < 1.5\Lambda_s$ and $\eta = \frac{1}{2}\ln\frac{t+x_L}{t-x_L} \simeq 0$:

$$\frac{dN}{d^2p_Td^2x_Td\eta} \equiv f(T_{\rm eff}) = \frac{a_1}{g^2}\left[\exp\left(\sqrt{p_T^2+m_{\rm eff}^2}/T_{\rm eff}\right)-1\right]^{-1}, \quad (7)$$

where $m_{\rm eff} = a_2\Lambda_{s0}$, $T_{\rm eff} = a_3\Lambda_s$; $a_2 = 0.0358$, $a_3 = 0.465$. The constant a_1/g^2 will be absorbed into factor ϵ_0, which is our fitting parameter.

The dependence of the distribution (7) on transverse coordinates $\mathbf{x}_T$ is constructed as follows [22]:

$$\Lambda_s^2(\mathbf{x}_T) = \Lambda_{s0}^2\frac{\rho(\mathbf{b},\mathbf{x}_T)}{\rho_0}, \quad (8)$$

where the participant density at a particular position in the transverse plane is defined by Eq. (3).

To define the initial energy density profile, we need the partonic phase-space distribution $f_0(x,p) = dN/d^3xd^3p$. Note that it is associated with the hypersurfaces $t = $ const. To express the phase-space density through the values $\frac{dN}{d^2x_Td^2pd\eta}$ defined at $\sqrt{t^2-x_L^2}=\tau_0$, one should take into account that the density of partons with momentum $\mathbf{p}$ crossing element $d^3\sigma(x)$ of this hypersurface is

$$p^0\left.\frac{dN}{d^3p}\right|_{d\sigma(x)} = p^\mu d\sigma_\mu(x) f_0(x,p) = f_0(x,p)\tau_0 p_T\cosh\theta d^2x_Td\eta, \quad (9)$$

where $\theta = y-\eta$ and y is the rapidity of partons (in momentum space). Therefore,

$$f_0(x,p) = \frac{1}{\tau_0 m_T\cosh\theta}\frac{dN}{d^2x_Td^2p_Td\eta dy}. \quad (10)$$

One can formally get the d^6N distribution from Eq. (7) by multiplying it by a δ function:

$$\frac{dN}{d^2p_Td^2x_Td\eta dy} = f(T_{\rm eff})\delta(y-\eta). \quad (11)$$

Such a phase-space distribution, corresponding the CGC asymptotic results [24], is widely used for a description of the initial state in $A+A$ collisions [25]. However, a presence of the δ function in the phase-space density contradicts evidently the basic principle of the quantum mechanics. Indeed, the classical phase-space density has to follow from the quantum mechanical one in some limit. The Wigner function $f_{\rm W}(x,p)$ [26], which is the quantum mechanical analog of the classical phase-space density $f(x,p)$, satisfies the restriction $\int f_{\rm W}^2(x,p)d^3pd^3x \leqslant (2\pi\hbar)^{-3}$ (see, for example, Ref. [27]; note that the equality takes place for a pure state only); here the normalization condition $\int f_{\rm W}(x,p)d^3pd^3x = 1$ is supposed. It evidently excludes utilization of the δ function as factor in the structure of the Wigner function. Therefore, to escape contradiction with quantum mechanics, an another prescription, instead of utilization of a δ function, should be used for the longitudinal part of distribution $f(x,p)$; it can be, for example, the boost-invariant prescriptions used in Ref. [17]. Following this recept, the smearing of δ function at hypersurface τ_0 in Eq. (11) is as follows:

$$\frac{dN}{d^2p_Td^2x_Td\eta dy} = f\left[\frac{T_{\rm eff}}{\cosh(\eta-y)}\right]. \quad (12)$$

In this way, we fix the phase-space density (10). This may correspond to quasithermal averaged partonic distribution, which can be reached at moment τ_0 owing to quantum effects (uncertainly principle), different kinds of turbulences, and the Schwinger-like mechanism of pair production in the pulse of a strong color field. It does not mean that the true thermalization that should be supported by a permanent mechanism of partonic interactions is reached at $\tau_0 \approx 3/\Lambda_s \approx 3$ fm/c.

As a result, we use the following form of boost-invariant phase-space distribution for gluons at the initial hypersurface τ_0:

$$f_0 = g^{-2}\frac{a_1(\tau_0 m_T\cosh\theta)^{-1}}{\exp\left[\sqrt{m_{\rm eff}^2(\mathbf{x}_T)+p_T^2}\cosh\theta/T_{\rm eff}(\mathbf{x}_T)\right]-1}, \quad (13)$$

where $\theta = \eta - y$, $\mathbf{x}_T = (X,Y) = (x_T\cos\varphi, x_T\sin\varphi)$, and we consider gluons as massless particles, $m_T = p_T$. Such a distribution depends on the effective mass $m_{\rm eff}(\mathbf{x}_T) = a_2\Lambda_s(\mathbf{x}_T)$ and the temperature $T_{\rm eff}(\mathbf{x}_T) = a_3\Lambda_s(\mathbf{x}_T)$ [numerical values for a_2 and a_3 are the same as in Eq. (7)], which, in accordance with Ref. [22], are determined by the local scale $\Lambda_s(\mathbf{x}_T)$ (8).

The components of the energy-momentum tensor in the pseudo-Cartesian coordinates reads

$$T^{\mu\nu}(x) = \int p^\mu p^\nu f(x,p)p_Tdp_Tdyd\phi, \quad (14)$$

where the Lorentz-invariant integration measure d^3p/p_0 in the Cartesian variables is already rewritten in Björken variables as $p_T dp_T dy d\phi$.

We numerically calculate the components of the energy-momentum tensor with the distribution function, following from Eq. (13), at $\eta = 0$.

Note that, at $\tau = \tau_0$, the energy-momentum tensor takes the form

$$T_0^{\mu\nu}(\mathbf{x}_T, x_L = 0) = \frac{a_1}{g^2\tau_0}\Lambda_s^3(\mathbf{x}_T)t^{\mu\nu}, \tag{15}$$

where $t^{\mu\nu}$ are the constant coefficients fixed by the constants a_2 and a_3. Therefore, the energy profile in transverse plane at τ_0 in central collisions can be presented in the form [see Eq. (8)]

$$\epsilon(x_T) = \epsilon_0 \frac{\rho^{3/2}(0, x_T)}{\rho_0^{3/2}}, \tag{16}$$

where the number of participants is defined by Eq. (3). For the same reason as for the Glauber-like IC, we use the form of this profile to build the IC for hydrokinetic evolution at the thermalization time $\tau_i = 1$ fm/c. The maximal energy density ϵ_0 at (proper) time τ_i is the fitting parameter as in the case of the Glauber IC.

III. THE THERMAL MATTER IN $A + A$ COLLISION AND EQUATION OF STATE

Here we describe the matter properties and its thermodynamic characteristics, for example, EoS, which are necessary components of the HKM. We suppose that soon after thermalization the matter created in $A + A$ collisions at RHIC energies is in the QGP state. Also at time τ_i, there is a peripheral region with relatively small initial energy densities: $\epsilon(r) < 0.5$ GeV/fm^3. This part of the matter ("corona") does not transform into QGP and has no chance of being involved in thermalization process [28]. By itself, the corona gives no essential contribution to the hadron spectra [28]. One should consider it separately from the thermal bulk of the matter and should not include in hydrodynamic evolution. Therefore, we cut the initial Glauber or CGC-like profiles at $\epsilon(r) \leqslant 0.5$ GeV/fm^3 when we consider IC for hydrodynamic evolution of the system.

During the system evolution the QGP is cooling and finally transforms into a hadron phase, most probably, according to the crossover scenario. Such a transformation may occur in the 170–190 MeV temperature interval. At temperature $T = T_{\rm ch} \approx 165$ MeV, the chemical freeze-out happens, as seen in an analysis of the particle number ratios [29,30]. The conception of the chemical freeze-out means that at the temperatures $T \geqslant T_{\rm ch}$ the bulk of the expanding matter is in the local thermal and chemical equilibrium, while at $T < T_{\rm ch}$ the chemical composition becomes in some sense frozen: one can neglect the majority of inelastic reactions except for decays of resonances and recombination processes. The hadronic matter is not in chemical equilibrium in the latter thermodynamic region. Moreover, the hadronic medium gradually emits particles in this zone, thus loosing also the local thermal equilibrium. Therefore, one should consider in different ways the matter evolution in the two four-dimensional (4D) space-time zones separated by the 3D hypersurface corresponding to the isotherm $T = T_{\rm ch} \approx 165$ MeV. Let us describe the thermodynamic properties of matter in both of these regions.

A. The EoS in the equilibrated space-time domain

At high temperatures corresponding to the QGP phase and crossover transition to hadron phase, we use a realistic EoS [31] adjusted to the lattice QCD results for zero barionic chemical potential so that it is matched with an ideal chemically equilibrated multicomponent hadron resonance gas at $T_c = 175$ MeV. To take into account a conservation of the net baryon number, electric charge, and strangeness in the QGP phase, one has first to make corrections to thermodynamic quantities for nonzero chemical potentials. As it is proposed in Ref. [32], a modification of the EoS can be evaluated by using of the Taylor series expansion in terms of the light and strange quark chemical potentials, or analogously in baryon and strange hadronic chemical potentials:

$$\frac{p(T, \mu_B, \mu_S)}{T^4} = \frac{p(T, 0, 0)}{T^4} + \frac{1}{2}\frac{\chi_B}{T^2}\left(\frac{\mu_B}{T}\right)^2 + \frac{1}{2}\frac{\chi_S}{T^2}\left(\frac{\mu_S}{T}\right)^2 + \frac{\chi_{BS}}{T^2}\frac{\mu_B}{T}\frac{\mu_S}{T}. \tag{17}$$

The expansion coefficients χ_B and χ_S are, respectively, the baryon number and strangeness susceptibilities which are related to thermal fluctuations of baryon number and strangeness in a thermal medium at zero chemical potentials.

To obtain the EoS in the equilibrium zone we use the numerical results for χ_B and χ_S as a function of the temperature given in Ref. [32]. The values for the ratios μ_q/T in (17) during the system evolution can be determined approximately. If at some hypersurface corresponding to an isotherm, like at the chemical freeze-out hypersurface, the chemical potentials are uniform and the following ratios remain constant:

$$\frac{\mu_q}{T} = \text{const}_q, \quad \text{where} \quad q = B, S, E$$

during the chemically equilibrated isoentropic evolution of the Boltzmann massless gas. In our approximation we use these constraints and find the corresponding constants from the chemical potentials obtained together with $T_{\rm ch}$ from an analysis of the particle-number ratios. In concrete calculations we use the chemical freeze-out temperature $T_{\rm ch} = 165$ MeV, corresponding chemical potentials $\mu_B = 29$ MeV, $\mu_S = 7$ MeV, and $\mu_E = -1$ MeV, and the strangeness suppression factor $\gamma_S = 0.935$, which are dictated by 200 A GeV RHIC particle-number ratio analysis done in the statistical model [29,30].

B. The EoS in the chemically nonequilibrated domain

At the chemical freeze-out temperature $T_{\rm ch}$ the "lattice" EoS taken from [31] and corrected for nonzero chemical potentials is matched with good accuracy with an ideal Boltzmann hadronic resonance gas, which includes $N = 359$ hadron states made of u, d, and s quarks with masses up to 2.6 GeV. Essentially, we use the same particle set in the FASTMC

event generator [33]. Technically, in the numerical code, we input the corresponding N functions—the densities n_i of each hadron i and the equations for n_i already at the very beginning of the system evolution; however, these densities are meaningless in the QGP phase and their evaluation does not influence the system evolution in the equilibrated zone. These functions are brought into play at $T < T_{\rm ch}$. If this thermodynamic region would correspond to the complete conservation of the particle numbers, then, in addition to the energy-momentum conservation, one would account for the conservation equations for particle number flows in the form

$$\partial_\mu (n_i u^\mu) = 0, \quad i = 1 \cdots N. \tag{18}$$

In our problem, however, during the system evolution in the nonequilibrated zone $T < T_{\rm ch}$, the resonance decays have to be taken into account. The decay law in a homogeneous medium with $T \ll m_i$ (m_i is the resonances mass) implies a summing up of a decrease of the unstable ith particle number owing to decays and an increase because of decays of heavier jth resonance into the ith particle:

$$\frac{dN_i}{dt} = -\Gamma_i N_i + \sum_j b_{ij} \Gamma_j N_j, \tag{19}$$

where Γ_i is the total width of resonance i, $b_{ij} = B_{ij} M_{ij}$ denotes the average number of ith particles coming from an arbitrary decay of jth resonance, $B_{ij} = \Gamma_{ij}/\Gamma_{j,\rm tot}$ is the branching ratio, and M_{ij} is the number of ith particles produced in $j \to i$ decay channel. The set of N equations (19), solved together, takes into account all possible cascade decays $i \to j \to k \to \cdots$. This also conserves net charges—for example, baryon, electric charge, and strangeness—because the charges are conserved in resonance decay process. If one relates Eq. (19) to the fluid element of some volume ΔV moving with four-velocity u^μ, then a covariant relativistic extension of the decay law for a hydrodynamic medium leads to Eq. (18),

$$\partial_\mu [n_i(x) u^\mu(x)] = -\Gamma_i n_i(x) + \sum_j b_{ij} \Gamma_j n_j(x), \tag{20}$$

when one neglects a thermal motion of the resonance j, which can be justified because post (chemical) freeze-out temperatures are much less than the mass of the lightest known resonance. Also, Eq. (20) for the hydrodynamic evolution is written under supposition of an instant thermalization of the decay products, which is consistent with the ideal fluid approximation (mean free path is zero). In the kinetic part of the HKM we consider the next approximation when the nonequilibrium character of the distribution functions and the kinetics of resonance decays are taken into account. We also can approximately account for a recombination in the processes of resonance decays into expanding medium just by utilizing the effective decay width $\Gamma_{i,\rm eff} = \gamma \Gamma_i$ in Eq. (20). We use $\gamma = 0.75$ [34] for the resonances containing u and d quarks supposing thus that about 30% of such resonances are recombining during the evolution.

Equation (20), together with the hydrodynamic equations and the EoS, should give one the energy density and composition of the gas in each space-time point. To find the EoS $p = p(\epsilon, \{n_i\})$ for the mixture of hadron gases, we start with the expressions for energy density and particle density for the ith component of multicomponent Boltzmann gas:

$$\begin{aligned} \epsilon_i &= \frac{g_i}{2\pi^2} m_i^2 T [3T K_2(m_i/T) + m K_1(m_i/T)] \exp(\mu_i/T), \\ n_i &= \frac{g_i}{2\pi^2} m_i^2 T K_2(m_i/T) \exp(\mu_i/T). \end{aligned} \tag{21}$$

Then, the equation for the temperature is

$$\epsilon = 3nT + \sum_i n_i m_i \frac{K_1(m_i/T)}{K_2(m_i/T)}, \tag{22}$$

where $n = \sum_i n_i$. Having solved this equation numerically for given ϵ and $\{n_i\}$, we get the temperature and then find the pressure using a simple relation for multicomponent Boltzmann gas:

$$p = nT. \tag{23}$$

Equations (22) and (23) define $p = p(\epsilon, \{n_i\})$.

Thus, we follow the evolution of all N densities of hadron species in hydrocalculation and compute the EoS dynamically for each chemical composition of N sorts of hadrons in every hydrodynamic cell in the system during the evolution. Using this method, we do not limit ourselves to chemically frozen or equilibrated evolution, keeping nevertheless a thermodynamically consistent scheme.

As was mentioned earlier, we use the Boltzmann approximation in the EoS calculation to decrease computational time. However, for emission function and spectra calculation we use quantum Bose-Einstein/Fermi-Dirac distribution functions with chemical potentials calculated to give the same particle densities as in the Boltzmann case. We checked that the measure of relative divergence in the energy density if one uses the quantum distribution functions instead of the Boltzmann one is not bigger than 3% in the thermodynamic region, which actually contributes to the formation of hadronic spectra.

IV. KINETICS IN THE NONEQUILIBRIUM HADRONIC ZONE

To describe the nonequilibrium evolution and decay of a hadronic system, we start from the Boltzmann equations for the mixture of hadrons, most of which have finite lifetimes and decay widths compatible with particle masses. The set of such equations for i components of the hadron resonance gas, which account for the only binary interactions (elastic scattering) and resonance decays, is

$$\begin{aligned} &\frac{p_i^\mu}{p_i^0} \frac{\partial f_i(x,p)}{\partial x^\mu} \\ &\quad = G_i^{\rm scatt} - L_i^{\rm scatt}(x,p) + G_i^{\rm decay}(x,p) - L_i^{\rm decay}(x,p) \\ &\quad \equiv G_i(x,p) - L_i(x,p). \end{aligned} \tag{24}$$

Here we ignore the processes of resonance recombination, which is simpler to account for phenomenologically (see the previous section). The term *gain* (G) describes an income of the particles into phase-space point (x, p) owing to scatters and resonance decays. The term *loss* (L) is related to a decrease of particles in the vicinity of the phase space point

(x, p) owing to rescattering and decays of resonances. The loss term is proportional to the particle number density at point x, so $L_i^{\text{scatt}}(x, p) = f_i R_i$, $L_i^{\text{decay}}(x, p) = f_i D_i$, where R is the scattering rate and D is the decay rate. If one considers the equations for stable or quasistable particles, then $L_i^{\text{decay}}(x, p) = 0$ ($D_i \equiv 0$).

The method making it possible to find the emission function of the hadrons based on the Boltzmann equations in the (generalized) relaxation time approximation was proposed in Refs. [5,6]. Following to this method we put $J_i(x, p) \approx R_{i,\text{l.eq.}}(x, p)$ and $G_i \approx R_{i,\text{l.eq.}}(x, p) f_{i,\text{l.eq.}}(x, p) + G_i^{\text{decay}}(x, p)$. The quantity $R(x, p) = \tau_{\text{rel}}^{-1}(x, p)$ is the inverse relaxation time or collision rate in the global reference frame. Then,

$$\frac{p^\mu}{p^0}\partial_\mu f_i(x, p) = \left[f_i^{\text{l.eq.}}(x, p) - f_i(x, p)\right] R_i(x, p) + G_i^{\text{decay}}(x, p) - L_i^{\text{decay}}(x, p). \tag{25}$$

The explicit form of the $G_i^{\text{decay}}(x, p)$ term will be derived later. In the first approximation to hydrokinetic evolution, the parameters of the local equilibrium distribution function $f_{i,\text{l.eq.}}(x, p)$, for example, the temperature $T(x)$ and chemical potentials $\mu_i(x)$ are determined by the hydrodynamic evolution. The details of hydrodynamic approach used in the model are described in the next section.

A. Emission functions in hyperbolic coordinates and spectra formation

All our results are related to the very central rapidity interval, $y \approx 0$, and we will use the boost-invariant approach to describe strong longitudinal matter expansion observed at RHIC. For such an approach the hyperbolic coordinates in (t, x_L) directions are more suitable than the Cartesian ones. Then the kinetic equations take the form

$$\frac{1}{m_T \cosh y}\left(m_T \cosh\theta \frac{\partial}{\partial\tau} - \frac{m_T \sinh\theta}{\tau}\frac{\partial}{\partial\eta} + \vec{p}_T \frac{\partial}{\partial \vec{r}_T}\right) \times f_i(\tau, \theta, \mathbf{r}_T, \mathbf{p}_T) = \left[f_i^{\text{l.eq.}}(\tau, \theta, \mathbf{r}_T, \mathbf{p}_T) - f_i(\tau, \theta, \mathbf{r}_T, \mathbf{p}_T)\right] R_i(\tau, \theta, \mathbf{r}_T, \mathbf{p}_T) + G_i^{\text{decay}}(\tau, \theta, \mathbf{r}_T, \mathbf{p}_T), \tag{26}$$

where $\tau = \sqrt{t^2 - x_L^2}$ is a proper time, $m_T = \sqrt{m^2 + p_T^2}$ is a transverse mass, $\theta = \eta - y$, η is a space-time rapidity, defined before Eq. (7), and y is a particle rapidity.

The formal solutions of Eq. (26) correspond to the nonequilibrium distribution functions in expanding and decaying a multihadronic system:

$$f_i(\tau, \theta, \mathbf{r}_T, \mathbf{p}_T) = f_i^{\text{l.eq.}}\left[\tau_0, \theta^{(\tau_0)}(\tau), \mathbf{r}_T^{(\tau_0)}(\tau), \mathbf{p}_T\right] \times \exp\left\{-\int_{\tau_0}^{\tau} \tilde{R}_i\left[s, \theta^{(s)}(\tau), \mathbf{r}_T^{(s)}(\tau), \mathbf{p}_T\right] ds\right\} + \int_{\tau_0}^{\tau} d\lambda \left\{f_i^{\text{l.eq.}}\left[\lambda, \theta^{(\lambda)}(\tau), \mathbf{r}_T^{(\lambda)}(\tau), \mathbf{p}_T\right] \tilde{R}_i \times \left[\lambda, \theta^{(\lambda)}(\tau), \mathbf{r}_T^{(\lambda)}(\tau), \mathbf{p}_T\right] + \tilde{G}_i^{\text{decay}}\left[\lambda, \theta^{(\lambda)}(\tau), \mathbf{r}_T^{(\lambda)}(\tau), \mathbf{p}_T\right]\right\} \times \exp\left\{-\int_{\lambda}^{\tau} \tilde{R}_i\left[s, \theta^{(s)}(\tau), \mathbf{r}_T^{(s)}(\tau), \mathbf{p}_T\right] ds\right\}, \tag{27}$$

where $\tilde{R}_i(\lambda, \theta, \mathbf{r}_T, \mathbf{p}_T) = \frac{\cosh y}{\cosh\theta} R_i(\lambda, \theta, \mathbf{r}_T, \mathbf{p}_T)$ and $\tilde{G}_i^{\text{decay}}(\lambda, \theta, \mathbf{r}_T, \mathbf{p}_T) = \frac{\cosh y}{\cosh\theta} G_i^{\text{decay}}(\lambda, \theta, \mathbf{r}_T, \mathbf{p}_T)$.

Here we use the notation

$$\begin{cases} \sinh\theta^{(\tau_0)}(\tau) = \frac{\tau}{\tau_0}\sinh\theta \\ \mathbf{r}_T^{(\tau_0)}(\tau) = \mathbf{r}_T - \frac{\mathbf{p}_T}{m_T}\left(\tau\cosh\theta - \sqrt{\tau_0^2 + \tau^2\sinh^2\theta}\right). \end{cases} \tag{28}$$

The invariant value is $p^0 R_i(x, p) = p^{*0} R_i^*(x, p)$, where the asterisks * denote a value in the local rest frame of the fluid element at point x, so

$$\tilde{R}_i(x, p) = \frac{\cosh y}{\cosh\theta} R_i(x, p) = \frac{\cosh y}{\cosh\theta}\frac{p^\mu u_\mu}{p^0} R_i^*(p, T) = \frac{p^\mu u_\mu}{m_T \cosh\theta} R_i^*(p, T). \tag{29}$$

To connect the formal solution (27) with observables, for example, the particle spectrum, we use the equality

$$p^0 \frac{d^3 n}{d^3 p} = \frac{d^2 n}{2\pi p_T dp_T dy} = \int_{\sigma_{\text{out}}} d\sigma_\mu p^\mu f(x, p), \tag{30}$$

where σ_{out} is a "distant" hypersurface of large $\tau = \text{const}$, where all the interactions among hadrons are ceased.

In what follows we use the variable substitution in the first term of Eq. (27) describing the "initial emission,"

$$\begin{cases} \sinh\theta = \frac{\tau_0}{\tau}\sinh\theta' \\ \mathbf{r}_T = \mathbf{r}'_T + \frac{\mathbf{p}_T}{m_T}\left(\tau\cosh\theta - \sqrt{\tau_0^2 + \tau^2\sinh^2\theta}\right), \end{cases} \tag{31}$$

and the substitution,

$$\begin{cases} \sinh\theta = \frac{\lambda}{\tau}\sinh\theta' \\ \mathbf{r}_T = \mathbf{r}'_T + \frac{\mathbf{p}_T}{m_T}\left(\tau\cosh\theta - \sqrt{\lambda^2 + \tau^2\sinh^2\theta}\right), \end{cases} \tag{32}$$

in the second term of Eq. (27) related to the "four-volume emission." After transformation to new variables $\{\tau, \theta', \vec{r}'\}$, we arrive with the result

$$\begin{aligned} &\int_{\sigma_{\text{out}}} d\sigma_\mu p^\mu f(x, p) \\ &= \int_{\sigma_0} d\sigma_0^\mu p_\mu f_i^{\text{l.eq.}}(\tau_0, \theta', \mathbf{r}'_T, p) \times \exp\left\{-\int_{\tau_0}^{\infty} \tilde{R}_i\left[s, \theta^{(s)}(\tau_0), \mathbf{r}_T^{(s)}(\tau_0), \mathbf{p}_T\right] ds\right\} \\ &+ \int_{\tau_0}^{\tau} d\lambda \int_{\sigma(\lambda)} d\sigma_\mu(\lambda) p^\mu \left[f_i^{\text{l.eq.}}(\lambda, \theta', \mathbf{r}'_T, \mathbf{p}_T)\tilde{R}_i \times (\lambda, \theta', \mathbf{r}'_T, \mathbf{p}_T) + \tilde{G}_i^{\text{decay}}(\lambda, \theta', \mathbf{r}'_T, \mathbf{p}_T)\right] \\ &\times \exp\left\{-\int_{\lambda}^{\infty} \tilde{R}_i\left[s, \theta^{(s)}(\lambda), \mathbf{r}_T^{(s)}(\lambda), \mathbf{p}_T\right] ds\right\} \\ &= p^0 \frac{d^3 N}{d^3 p}, \end{aligned} \tag{33}$$

where $\sigma(\lambda)$ is $\tau = \lambda = \text{const}$ hypersurface, so $d\sigma_\mu(\lambda)p^\mu = \lambda m_T \cosh\theta' d\theta' d^2\vec{r}'_T$. The exponential values in these expressions are the escape probabilities

$$\mathcal{P}(\tau, \mathbf{r}_T, \theta, \mathbf{p}_T) = \exp\left\{-\int_\tau^\infty \tilde{R}_i\left[s, \theta^{(s)}(\tau), r_T^{(s)}(\tau), \mathbf{p}_T\right] ds\right\} \tag{34}$$

for particles with momentum p at space-time point $(\tau, \mathbf{r}_T, \eta = \theta + y)$ (in hyperbolic coordinates) to become free without any collision [5,6].

In the preceding expression we can separate the four-volume emission function

$$S_i(\lambda, \theta, \mathbf{r}_T, \mathbf{p}_T) = \left[f_i^{\text{l.eq.}}(\lambda, \theta, \mathbf{r}_T, p)\tilde{R}_i(\lambda, \theta, r_T, p) + \tilde{G}_i^{\text{decay}}(\lambda, \theta, \mathbf{r}_T, \mathbf{p}_T)\right]\mathcal{P}(\lambda, \mathbf{r}_T, \theta, \mathbf{p}_T) \tag{35}$$

and the initial emission:

$$S_{i,0}(\theta, \mathbf{r}_T, \mathbf{p}_T) = f_i^{\text{l.eq.}}(\tau_0, \theta, \mathbf{r}_T, \mathbf{p}_T)\mathcal{P}(\tau_0, \mathbf{r}_T, \theta, \mathbf{p}_T). \tag{36}$$

These expressions demonstrate obviously that the particle emission is formed by the particles that undergo their *last* interaction or are already free initially. These expressions for the hadron emission function are the basic functions for calculations of the single- and multiparticle spectra [5]. To evaluate these quantities for observed (quasi-) stable particles, one needs to find the term gain G_i^{decay} for resonance decays and the collision rates R_i.

B. Resonance decays in multicomponent gas

We suppose that in the first (hydrodynamic) approximation the products of resonance decays that interact with the medium are thermalized and they become free later, after the last collision with one of other particles. However, at the late stages of matter evolution the system becomes fairly dilute, so that some of these produced particles get a possibility to escape without any collisions: $\mathcal{P} > 0$. To describe this we use the following forms for L_i^{decay} and G_i^{decay} terms (for two-particle resonance decay) [35]:

$$p_i^0 L_i^{\text{decay}}(x, p_i) = \sum_k \sum_l \int \frac{d^3p_k}{p_k^0} \int \frac{d^3p_l}{p_l^0} \Gamma_{i\to kl} f_i(x, p_i) \times \frac{m_i}{F_{i\to kl}} \delta^{(4)}(p_i - p_k - p_l) = m_i \Gamma_i f_i(x, p_i), \tag{37}$$

where resonance i decays into particles or resonances k and l,

$$p_i^0 G_i^{\text{decay}}(x, p_i) = \sum_j \sum_k \int \frac{d^3p_j}{p_j^0} \int \frac{d^3p_k}{p_k^0} \Gamma_{j\to ik} f_j(x, p_j) \times \frac{m_j}{F_{j\to ik}} \delta^{(4)}(p_j - p_k - p_i), \tag{38}$$

where the resonance j decays into particles i and k with partial width $\Gamma_{j\to ik}$ for this decay channel, and

$$F_{j\to ik} = \int \frac{d^3p_k}{p_k^0} \int \frac{d^3p_i}{p_i^0} \delta^{(4)}(p_j - p_k - p_i) = \frac{2\pi}{m_j^2}\left[\left(m_j^2 - m_k^2 - m_i^2\right)^2 - 4m_i^2 m_k^2\right]^{1/2}. \tag{39}$$

To escape the complicated problem with satisfaction of thermodynamic identities in hadron resonance gas, we utilize in what follows the mass shell approximation for resonances, supposing that $m_i = \langle m_i \rangle$. Also, as it was already discussed, we take into account that the resonance mass in hadron resonance gas is much larger than the temperature, $m_i \gg T_c$. Then the most probable velocity of resonance in the rest system of a fluid element is small, $\overline{v}_i \approx \sqrt{\frac{2T}{m_i}}$, and one can use the approximation

$$p_i^\mu \approx m_i u^\mu. \tag{40}$$

So the resonance distribution function takes the form

$$f_j(x, p_i) \approx \frac{p_j^0}{m_j} n_j(x) \delta^3[\mathbf{p}_j - m_j \mathbf{u}(x)]. \tag{41}$$

It allows us to perform integrations in Eq. (38) over p_j, p_k analytically and get

$$G_i^{\text{decay}}(x, p_i) = \sum_j \sum_k \Gamma_{j\to ik} \frac{n_j(x)}{p_i^0 p_k^0 F_{j\to ik}} \delta \times \left[m_j u^0(x) - p_k^0 - p_i^0\right], \tag{42}$$

where $p_k^0 = \sqrt{m_k^2 + [m_j \mathbf{u}(x) - \mathbf{p}_i]^2}$.

Just this form of gain term is used when spectra are evaluated according to Eq. (33). Note that in practical calculations we substitute the δ function with its Gaussian representation,

$$\delta(x) = \frac{1}{R\sqrt{\pi}} e^{-x^2/R^2},$$

and take a finite parameter value $R = 50$ MeV.

C. Collision rates

The collision rate $R(x, p) = \frac{1}{\tau_{\text{rel}}(x,p)}$ is one of the basic values for calculating the intensity of the interactions in the expanding system and its decoupling. The latter is described through the escape probability $\mathcal{P}(x, p)$ (34)—the integral value of R along the possible trajectory of a particle with momentum p running freely through the whole expending system. The rate of collisions in the rest frame of some fluid element that accounts for scatters of a given particle with any other ith hadronic species in the thermal Boltzmann system depends only on particle energy $E_p^* = p^\mu u_\mu$ and the thermodynamic parameters of this fluid element [36]:

$$R^*(E_p^*, T, \{\mu_i\}) = \sum_i \int d^3k_i \frac{g_i}{(2\pi)^3} \exp\left[-\frac{E_{k,i} - \mu_i(x)}{T(x)}\right] \times \sigma_i(s_i) \frac{\sqrt{[s_i - (m - m_i)^2][s_i - (m + m_i)^2]}}{2E_p^* E_{k,i}}. \tag{43}$$

Here $g_i = (2j_i + 1)$, $E_p = \sqrt{\mathbf{p}^{*2} + m^2}$, $E_{k,i} = \sqrt{\mathbf{k}_i^2 + m_i^2}$, $s_i = (p^* + k_i)^2$ is the squared c.m. energy of the pair, and $\sigma_i(s)$ is the total cross section of selected particle with particle i in the corresponding binary collision. One can change the integration variable to squared c.m. energy s, energy of scattering partner E_k, and momentum angle ϕ, and perform E_k and ϕ integration analytically, which gives the following expression for the remaining integral:

$$\begin{aligned} &R^*(E_p^*, T, \{\mu_i\}) \\ &= \sum_i \frac{g_i T e^{\mu_i/T}}{8\pi^2 p^* E_p^*} \int_{(m+m_i)^2}^{\infty} ds \sigma_i(s) \\ &\times \sqrt{\left(s - m^2 - m_i^2\right)^2 - 4m_i^2 m^2} \\ &\times \sinh\left[\frac{p*}{2Tm^2}\sqrt{\left(s - m^2 - m_i^2\right)^2 - 4m_i^2 m^2}\right] \\ &\times \exp\left[-\frac{\left(s - m^2 - m_i^2\right)E_p^*}{2Tm^2}\right]. \end{aligned} \tag{44}$$

We calculate $\sigma_i(s)$ in a way similar to the UrQMD code [37]:

(i) The Breit-Wigner formula is applied for meson-meson and meson-baryon scattering:

$$\begin{aligned} \sigma_{\text{total}}^{\text{MB}}(\sqrt{s}) = &\sum_{R=\Delta,N^*} \langle j_B, m_B, j_M, m_M \| J_R, M_R \rangle \\ &\times \frac{2S_R + 1}{(2S_B + 1)(2S_M + 1)} \\ &\times \frac{\pi}{p_{cm}^2} \frac{\Gamma_{R\to\text{MB}}\Gamma_{\text{total}}}{(M_R - \sqrt{s})^2 + \Gamma_{\text{tot}}^2/4}, \end{aligned}$$

where $\Gamma_{\text{total}} = \sum_{(\text{channels})} \Gamma_{R\to\text{MB}}$, with $\sqrt{s}$-dependent parametrization of partial decay widths,

$$\begin{aligned} \Gamma_{R\to\text{MB}}(M) = \Gamma_R \frac{M_R}{M} &\left[\frac{p_{\text{CMS}}(M)}{p_{\text{CMS}}(M_R)}\right]^{2l+1} \\ &\times \frac{1.2}{1 + 0.2\left[\frac{p_{\text{CMS}}(M)}{p_{\text{CMS}}(M_R)}\right]^{2l}}, \end{aligned}$$

chosen to depend on absolute value of particle momentum in two-particle rest frame:

$$p_{\text{CMS}}(\sqrt{s}) = \frac{1}{2\sqrt{s}}\sqrt{\left(s - m_1^2 - m_2^2\right)^2 - 4m_1^2 m_2^2}.$$

In the case of meson-meson scattering, a constant elastic cross section of 5 mb is added to fully reproduce the measured cross section.

(ii) Particle Data Group table data for $p - p$, $p - n$, $p - \bar{p}$, etc., scattering is used.

(iii) For other baryon-baryon scattering, an additive quark model,

$$\begin{aligned} \sigma_{\text{total}} = 40 &\left(\frac{2}{3}\right)^{m_1+m_2} \left(1 - 0.4\frac{s_1}{3 - m_1}\right) \\ &\times \left(1 - 0.4\frac{s_2}{3 - m_2}\right) [\text{mb}], \end{aligned}$$

where $m_i = 1(0)$ corresponds to meson(baryon) and s_i is the number of strange quarks in hadron i, is used.

Note that all relevant resonance states (see preceding)—359 different species—are taken into account for the calculation of $\sigma_i(s)$.

V. HYDRODYNAMICS

We describe the system evolution in the equilibrium zone at $T > T_{\text{ch}}$ by the perfect hydrodynamics. The small shear viscosity effects, which lead to an increase of the transverse flows [10] we account for phenomenologically, including this effect in the parameter α of initial velocity as described in Sec. II A. The matter evolution in this zone is described by the relativistic hydrodynamical equations related to the conservation of energy momentum,

$$\partial_\nu T^{\mu\nu} = 0, \tag{45}$$

and equations associated with the net baryon number, strangeness, and isospin conservations

$$\partial_\nu (q_i u^\nu) = 0. \tag{46}$$

Here q_i is the density of the conserved quantum number.

At $T < T_{\text{ch}}$ the equations for the system evolution in the first approximation, $f_i = f_i^{l.eq}$, can be derived from the basic equation (25). Namely, integrating the left- and right-hand sides of Eq. (25) over d^3p, one arrives at Eq. (20) for particle number flow in the nonequilibrium zone and at hydrodynamic equation (45) by integrating Eq. (25) over $p_i^\nu d^3 p_i$ and summing over index i.

Note that in the first approximation the matter evolution is described by the equations of ideal hydrodynamics while the distribution function (27) in a decaying system is in nonequilibrium. The iteration procedure, including the next-order approximations, which, in fact, leads to viscous hydrodynamic evolution, is described in Ref. [6]. In this article we limit ourselves with the first approximation. Then the energy-momentum tensor $T^{\mu\nu}$ has a simple structure, which is employed in this model,

$$T^{\mu\nu} = (\epsilon + p)u^\mu u^\nu - p \cdot g^{\mu\nu}, \tag{47}$$

where ϵ is energy density and p is pressure defined from the EoS. In the chemically equilibrated zone the pressure is defined from the lattice QCD calculations, as discussed in Sec. III A. In the nonequilibrium zone the EoS generally depends on all 360 variables, $p = p(\epsilon, \{n_i\})$, and it is evaluated altogether with solution of the evolutionary equations. The reason is that it is impossible to store the EoS table; therefore, we compute pressure each time we need to (e.g., when restoring thermodynamic variables from conservative variables or when computing fluxes through each cell boundary) solving analytic Eqs. (22) and (23) numerically.

Let us rewrite equations in hyperbolic coordinates. These coordinates are suitable for dynamical description at RHIC energies, because, for example, zero longitudinal flows correspond to boost-invariant expansion (so nonzero longitudinal flow corresponds to deviation from boost invariance), and

evolution parameter $\tau = \sqrt{t^2 - x^2}$ is not affected by strong longitudinal flow, which saves computational time. It is convenient to write the equations in conservative form; then the conservative variables are

$$\vec{Q} = \begin{pmatrix} Q_\tau \\ Q_x \\ Q_y \\ Q_\eta \\ \{Q_{n_i}\} \end{pmatrix} = \begin{pmatrix} \gamma^2(\epsilon + p) - p \\ \gamma^2(\epsilon + p)v_x \\ \gamma^2(\epsilon + p)v_y \\ \gamma^2(\epsilon + p)v_\eta \\ \{\gamma n_i\} \end{pmatrix}. \tag{48}$$

Here the expression in curly brackets denotes N variables associated with the particle densities for each sort of hadron. The Q_i are conservative variables in the sense that an integral (discrete sum over all cells) of Q_i gives the total energy, momentum, and particle numbers, which are conserved up to the fluxes on the grid boundaries. The velocities in this expression are defined in a LCMS (longitudinally comoving system) and related to velocities in the laboratory frame as

$$\begin{aligned} v_x &= v_x^{\text{lab}} \cdot \frac{\cosh y_f}{\cosh(y_f - \eta)}, \\ v_y &= v_y^{\text{lab}} \cdot \frac{\cosh y_f}{\cosh(y_f - \eta)}, \\ v_\eta &= (y_f - \eta), \end{aligned} \tag{49}$$

where $y_f = \frac{1}{2}\ln[(1 + v_z^{\text{lab}})/(1 - v_z^{\text{lab}})]$ is the longitudinal rapidity of fluid element, $\eta = \frac{1}{2}\ln[(t + z)/(t - z)]$ is the geometrical rapidity.

The full hydrodynamical equations are

$$\underbrace{\partial_\tau \begin{pmatrix} Q_\tau \\ Q_x \\ Q_y \\ Q_\eta \\ \{Q_{n_i}\} \end{pmatrix}}_{\text{quantities}} + \vec{\nabla} \cdot \underbrace{\begin{pmatrix} Q_\tau \\ Q_x \\ Q_y \\ Q_\eta \\ \{Q_{n_i}\} \end{pmatrix} \vec{v} + \begin{pmatrix} \vec{\nabla}(p \cdot \vec{v}) \\ \partial_x p \\ \partial_y p \\ \frac{1}{\tau}\partial_\eta p \\ 0 \end{pmatrix}}_{\text{fluxes}} + \underbrace{\begin{pmatrix} (Q_\tau + p)\big(1 + v_\eta^2\big)\big/\tau \\ Q_x/\tau \\ Q_y/\tau \\ 2Q_\eta/\tau \\ \{Q_{n_i}/\tau\} \end{pmatrix}}_{\text{sources}} = 0 \tag{50}$$

and $\vec{\nabla} = (\partial_x,\ \partial_y,\ \frac{1}{\tau}\partial_\eta)$.

For hydrodynamic calculations related to the midrapidity region on central $A + A$ collisions, we impose longitudinal symmetry and cylindrical symmetry in transverse direction. This actually means that tangential (in transverse direction) and longitudinal velocities in LCMS vanish, so $Q_\phi = Q_\eta = 0$, as well as the fluxes in the ϕ and η directions. Then, one has to solve the following set of equations:

$$\underbrace{\partial_\tau \begin{pmatrix} Q_\tau \\ Q_r \\ \{Q_{n_i}\} \end{pmatrix}}_{\text{quantities}} + \partial_r \cdot \underbrace{\begin{pmatrix} (Q_\tau + p)v_r \\ Q_r v_r + p \\ \{Q_{n_i} v_r\} \end{pmatrix}}_{\text{fluxes}} + \underbrace{\begin{pmatrix} (Q_\tau + p)(1 + v_\eta^2)\big/\tau - (Q_\tau + p)v_r/r \\ Q_r/\tau - Q_r v_r/r \\ \{Q_{n_i}/\tau - Q_{n_i} v_r/r\} \end{pmatrix}}_{\text{sources}} = 0. \tag{51}$$

v_r/r is practically ambiguous at $r = 0$, so we put $v_r/r = \alpha$ there and use α value interpolated from the neighboring points.

We base our calculations on the finite-volume approach: We discretize the system on a fixed grid in the calculational frame and interpret Q_i^n as average value over some space interval i, which is called a cell (i is a multi-index in multidimensional case). We also split continuous time evolution into a sequence of finite time steps n.

The Q_i^n are then updated after each time step according to the fluxes on the cell interface during the time step Δt_n. In the 3D case, one has the following update formula:

$$\begin{aligned} Q_{ijk}^{n+1} = Q_{ijk}^n &- \frac{\Delta t}{\Delta x_1}(F_{i+1/2,jk} + F_{i-1/2,jk}) \\ &- \frac{\Delta t}{\Delta x_2}(F_{i,j+1/2,k} + F_{i,j-1/2,k}) \\ &- \frac{\Delta t}{\Delta x_3}(F_{ij,k+1/2} + F_{ij,k-1/2}), \end{aligned} \tag{52}$$

where F is the average flux over the cell boundary and indexes $+1/2$ and $-1/2$ correspond to right and left cell boundary, respectively, in each direction.

This is a basis of the Godunov method [38], which implies that the distributions of variables on the grid are piecewise. This forms the Riemann problem at each cell interface. Then the flux through each cell interface depends only on the solution of a single Riemann problem, supposing that the waves from the neighboring discontinuities do not intersect. The latter is satisfied with Courant-Friedrichs-Lewy condition [39].

To solve the Riemann problems at each cell interface, we use relativistic Harten-Lax-van Leer-Einfeldt solver [40], which approximates the wave profile in the Riemann problem with a single intermediate state between two shock waves propagating away from the initial discontinuity. Together with the shock-wave-velocity estimate, in this approximation one can obtain analytical dependence of flux on initial conditions for the Riemann problem, which makes the algorithm explicit.

We proceed then to construct a higher-order numerical scheme. To do so,

(i) in time: the *predictor-corrector* scheme is used for the second order of accuracy in time; that is, the numerical error is $O(dt^3)$ instead of $O(dt^2)$;

(ii) in space: in the same way, to achieve the second-order scheme, the *linear distributions* of quantities (conservative variables) inside cells are used.

A. Multidimension problem

At each time step, we compute and sum the fluxes for each cell with those of all its neighbors and update the value of conservative variables with the total flux. Thus, we do not use operator splitting (dimensional splitting) and thus avoid the numerical artifacts introduced by this method, for example, artificial spatial asymmetry.

B. Grid boundaries

To treat grid boundaries, we use the method of *ghost cells*. We include the two additional cells on either end of grid in each direction and set the quantities in these cells at the beginning of each time step. For simplicity, we set the quantities in ghost cells to be equal to these in the nearest "real" cell, thus implementing nonreflecting boundary conditions (outflow boundary). This physically corresponds to the boundary, which does not reflect any wave, which is consistent with expansion into vacuum.

C. Vacuum treatment

In our simulations we deal with spatially finite systems expanding into vacuum. Thus, computational grid in the Eulerian algorithm must initially contain both system and surrounding vacuum. To account for a finite velocity of expansion into vacuum, which equals c for an infinitesimal slice of matter on the boundary, we introduce additional (floating-point) variables in each cell, which keep the extent of matter expansion within a cell, having value 1 for the complete cell and 0 for a cell with vacuum only. The matter is allowed to expand in the next vacuum cell only if the current cell is filled with the matter.

VI. RESULTS AND DISCUSSION

In this article we apply the HKM for an analysis of the space-time picture of Au + Au collisions at the top RHIC energies. Such an analysis provided in the evolutionary models of heavy-ion collisions have to be based on a detailed description of the pion and kaon femtoscopic scales and must also describe well the *absolute* values of the spectra (not only spectra slopes) of the particles. As was noted in Ref. [6], the following factors favor the simultaneous description of the mentioned data: a relatively hard EoS (crossover transition between hadronic and quark-gluon matters, not the first-order phase transition), the pre-thermal transverse flows developed to thermalization time, an account for an "additional portion" of the transverse flows owing to the shear viscosity effect [10], a correct description of the gradual decay of the system at the late stage of the expansion. All these factors are included in the presented version of the HKM.

We use both the Glauber-like (Sec. II A) and the CGC-like (Sec. II C) initial conditions. In the former case the mean transverse radii, defined by Eq. (1), is $R_T = 4.137$ fm for the top RHIC energy. The best fit for the Glauber IC is reached at the following values of the two fitting parameters related to the proper time $\tau = 1$ fm/c: $\epsilon_0 = 16.5$ GeV/fm^3 ($\langle\epsilon\rangle = 11.69$ GeV/fm^3) and parameter of the initial velocity defined by Eq. (1), $\alpha = 0.248$ ($\langle v_T\rangle = 0.224$). In the case of the CGC-like initial conditions $R_T = 3.88$ fm, the fitting parameters leading to the best data description are $\epsilon_0 = 19.5$ GeV/fm^3 ($\langle\epsilon\rangle = 13.22$ GeV/fm^3) and $\alpha = 0.23$ ($\langle v_T\rangle = 0.208$). The parameters α for the initial transverse flows are somewhat larger than they are for the free streaming approximation of the prethermal stage [17]. The reason is, as it is explained in Sec. II, that the fitting parameter α is related to the "unknown portions" of flows, caused by the two factors: a developing of the prethermal flows and the viscosity effects in the QGP. In addition, an account of the event-by-event fluctuations of the initial conditions also leads to an increase of the "effective" transverse flows, obtained by averaging at the final stage, as compared to the results based on the initial conditions averaged over initial fluctuations [41]. Because we use the later kind of IC, it should lead also to an increase of the effective parameter α.

As was discussed in Sec. III, the chemically nonequilibrated evolution at the late stage, $T < T_{\rm ch} = 165$ MeV is not characterized by a simple EoS, like $p = p(\epsilon, \mu_B)$. In our calculations the pressure in this domain depends on 360 variables: energy density and particle concentrations. In Fig. 1 we illustrate the "effective" EoS at the temperatures around and below $T_{\rm ch}$. The points related to the later region characterize all diapasons that the pressure gains at each energy density when the system evolves with the Glauber IC fixed above. We see that the pressure is different from that in the "limited" cases: the chemically equilibrated and completely chemically frozen evolution [when the numbers of *all* (quasi) stable particles and resonances are conserved]. At relatively large energy densities in a

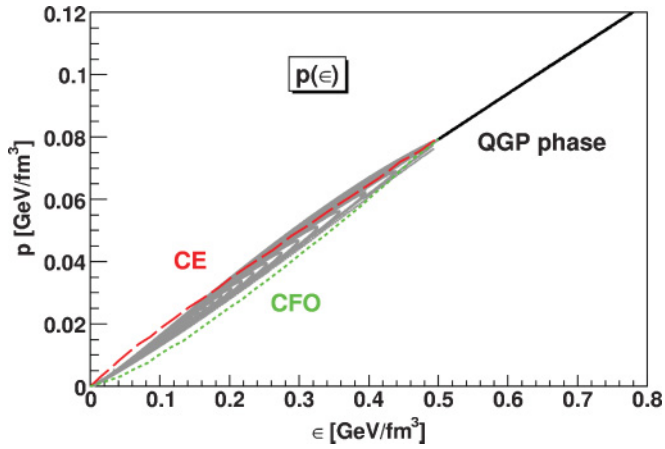

FIG. 1. (Color online) EoS $p(\epsilon)$ used in the HKM calculations. The solid black line is related to the chemically equilibrated phase, taken from lattice QCD results as described in Sec. III A, while gray region consists of the set of the points corresponding to the different hadron gas compositions at each ϵ occurring during the late nonequilibrium stage of the evolution. The dashed line denotes EoS for the chemically equilibrated hadron gas, and the dotted line denotes that for the chemically frozen one. They are shown for a comparison.

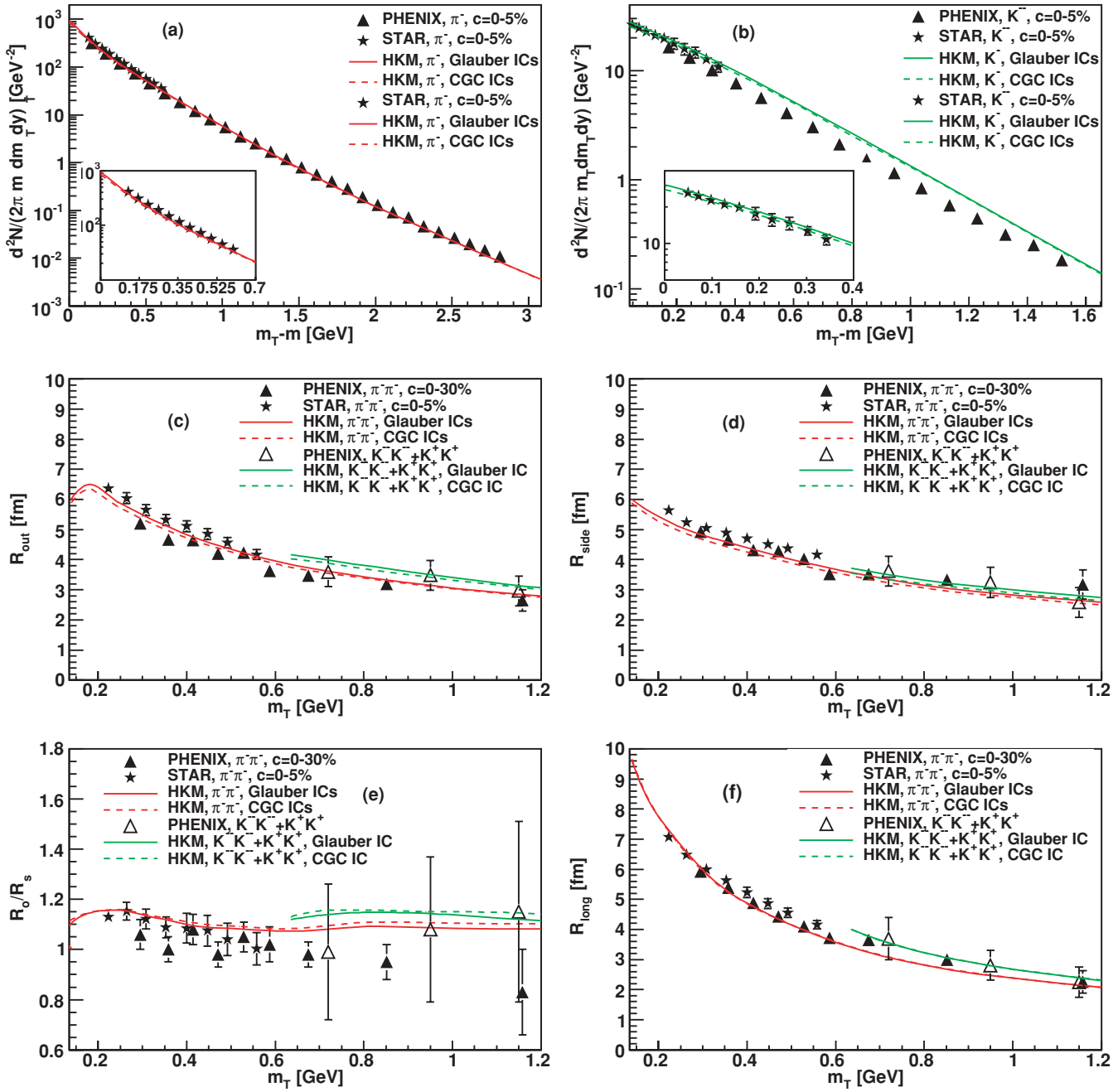

FIG. 2. (Color online) The transverse momentum spectra of (a) negative pions and (b) negative kaons, all calculated in the HKM model. The comparison only with the STAR data are presented in the separate small plots. The interferometry radii (c) $R_{\rm out}$, (d) $R_{\rm side}$ and (f) $R_{\rm long}$ and (e) $R_{\rm out}/R_{\rm side}$ ratio for $\pi^-\pi^-$ pairs and mixture of K^-K^- and K^+K^+ pairs. The experimental data are taken from the STAR [44,45] and PHENIX [46–48] Collaborations.

dominated space-time region the nonequilibrium EoS is harder than even in the chemically equilibrated case. This could reduce the out-to-side ratio for transverse interferometry radii.

The results of the HKM for the pion and kaon spectra, interferometry radii and $R_{\rm out}/R_{\rm side}$ ratio, are presented in Fig. 2. Because the temperature and baryonic chemical potential at chemical freeze-out, which are taken from the analysis of the particle number ratios [29], are more suitable for the STAR experiment, the HKM results for kaon spectra are good for the STAR data but not so much for the PHENIX ones. Note also that, in spite of other studies (e.g., [4]), we compare our results for the interferometry radii within the whole measured interval of p_T covered at the top RHIC energy. Finally, one can conclude from Fig. 2 that the description of pion and kaon spectra and space-time scales is quite good for both IC, the Glauber and CGC. It is worth noting, however, that the two fitting parameters α and ϵ_0 are various by 10–20% for different IC, as is described above.

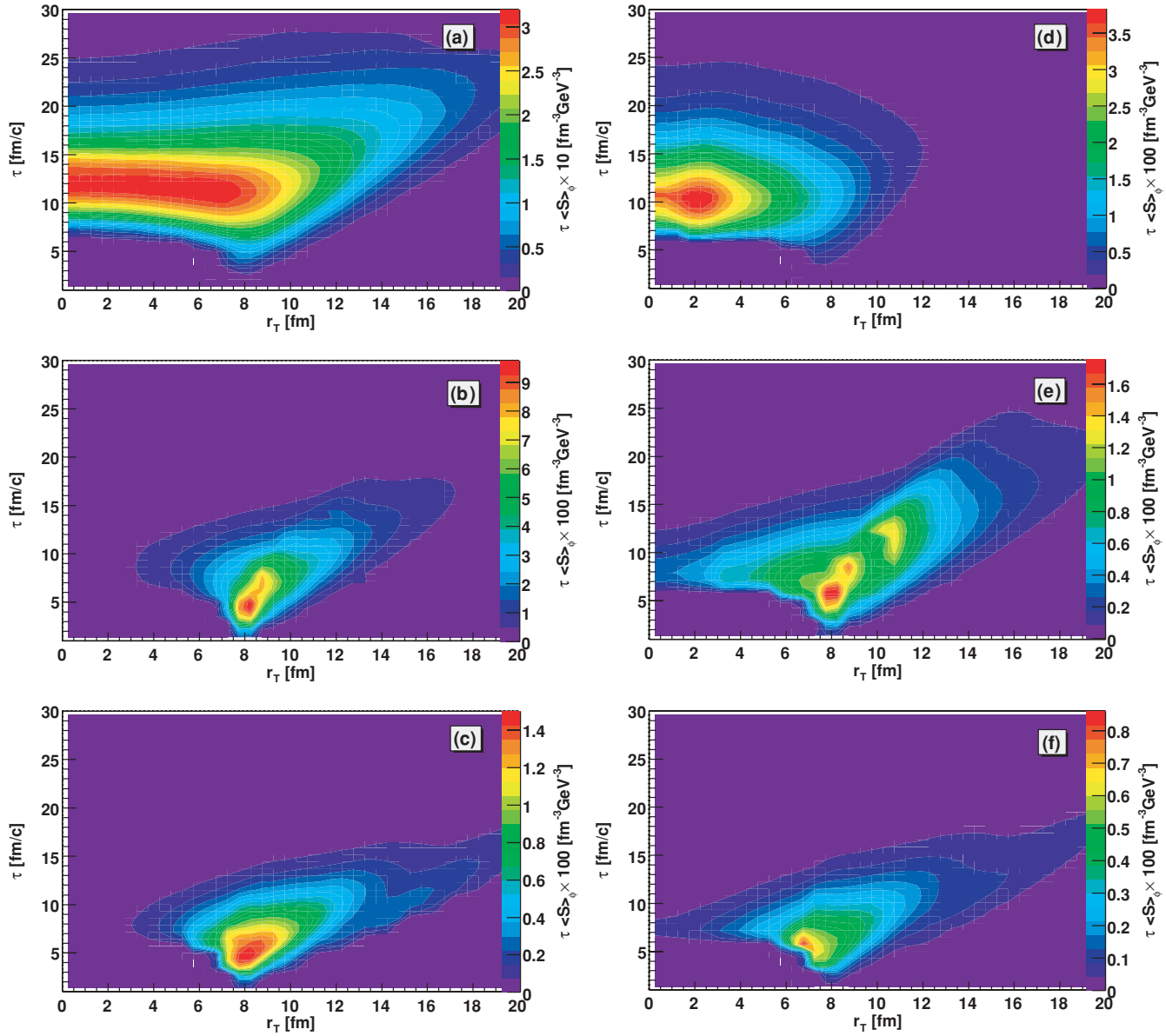

FIG. 3. (Color online) The ϕ_p-integrated emission functions of (a,b,c) negative pions and (d,e,f) negative kaons with different momenta: (a,d) $p_T = 0.2$ GeV, (b) $p_T = 0.85$ GeV, (e) $p_T = 0.7$ GeV, and (c,f) $p_T = 1.2$ GeV at the Glauber IC. The values of p_T in the middle row (b,e) correspond to the same transverse mass for pions and kaons $m_T = 0.86$ GeV.

The special attention acquires a good description of the pion and kaon longitudinal radii together with the $R_{\rm out}/R_{\rm side}$ ratio, practically, within the experimental errors. Such an achievement means that the HKM catches the main features of the matter evolution in $A + A$ collisions and correctly reproduces the homogeneity lengths in the different parts of the system that are directly related to the interferometry radii at the different momenta of the pairs [2]. In this connection it is valuable to show the structure of the emission function for pions and kaons.

In Fig. 3 we illustrate the space-time structure of the particle emission at the Glauber IC for different transverse momenta of particles, with the longitudinal momenta close to zero. The space-time picture of particle liberation is quite different for different transverse momenta: For the soft particles the maximal emission occurs close to the cental part and happens at relatively later times, while the most of the hard particles are emitted from the periphery of the system at early times. In fact (see also Refs. [6,42]), the temperatures in the regions of the maximal emission are quite different for different p_T; they are for pions $T \approx 75$–110 MeV for $p_T = 0.2$ GeV/c and $T \approx 130$–135 MeV for $p_T = 1.2$ GeV/c. So, if one uses the generalized Cooper-Frye prescription [6,42] applied to the *hypersurfaces of the maximal emission*, these hypersurfaces will be different for the different particle momenta and do not correspond to common isotherm [6,42].

One can see in Fig. 3 (top panels) that at *equal* transverse momentum p_T the maximal emission of kaons happens earlier

than pions, as one can expect because the kaons interact more weakly. At the same time the kaon interferometry radii in Fig. 2 follow approximately to the pion radii, demonstrating the approximate m_T scaling [43] with deviations to the slightly larger values than pion radii have. Explanations can be gained from the middle row in Fig. 3, where the comparison is done for the same transverse mass of pions and kaons. Then the maxima of pion and kaon emissions become closer and the majority of kaons leave system even somewhat later than pions at the same m_T, opposite to the comparison at the same p_T. Because in the simplest situations the homogeneity lengths for bosons depend on m_T [43], one could say that the approximate m_T scaling could indicate the similarity of the freeze-out picture for kaons and pions. However, probably, such a conclusion is very approximate because the real structure of the emission processes in $A + A$ collisions is quite complicated, as one can see from the details in Fig. 3.

VII. CONCLUSIONS

The HKM [5,6] is developed for a detailed study of the matter evolution and space-time picture of hadronic emission from rapidly expanding fireballs in $A+A$ collisions. The model allows one to describe the evolution of the QGP, as well as the gradually decoupling hadronic fluid—a chemically nonequilibrium matter, where the EoS is defined at each space-time point and accounts for decays of resonances into the nonequilibrated medium.

The HKM is applied to restore the initial conditions and space-time picture of the matter evolution in central Au + Au collisions at the top RHIC energy. The analysis, which is based on a detailed reproduction of the pion and kaon momentum spectra and measured femtoscopic scales, demonstrates that basically the pictures of the matter evolution and particle emission are similar at both Glauber and CGC IC with, however, different initial maximal energy densities: It is about 20% more for the CGC initial conditions. The initial prethermal flow is slightly less for the CGC IC. The main factors, which allow one to describe well simultaneously the spectra and femtoscopic scales, are a relatively hard EoS (crossover transition and chemically nonequilibrium composition of hadronic matter), prethermal transverse flows developed to thermalization time, an account for an "additional portion" of the transverse flows owing to the shear viscosity effect and fluctuation of initial conditions, and a correct description of a gradual decay of the nonequilibrium fluid at the late stage of expansion. Then one does not require the too-early thermalization time, $\tau_i < 1$ fm/c, to describe the data well. All these factors are included in the presented version of the HKM and it allows one to describe observables with only the two parameters.

An analysis of the emission function at the top RHIC energies demonstrates that the process of decoupling the fireballs created in Au + Au collision lasts from about 8 to 20 fm/c, more than half the fireball's total lifetime. The temperatures in the regions of the maximal emission are different at the different transverse momenta of emitting pions: $T \approx 75$–110 MeV for $p_T = 0.2$ GeV/c and $T \approx 130$–135 MeV for $p_T = 1.2$ GeV/c. A comparison of the pion and kaon emissions at the same transverse mass demonstrates the similarity of the positions of emission maxima, which could point out to the reason for an approximate m_T scaling.

VIII. SUMMARY

The advanced HKM tool allows one to describe the process of fireball evolution and gradual particle liberation in agreement with underlying kinetic equations. Further developments of the hydrokinetic approach and an analysis of the data in noncentral $A + A$ collisions will be the subject of a follow-up work.

ACKNOWLEDGMENTS

The authors thank S. V. Akkelin for fruitful discussions. The research was carried out within the scope of the EUREA: European Ultra Relativistic Energies Agreement (European Research Group: Heavy ions at ultrarelativistic energies) and is supported by the Fundamental Researches State Fund of Ukraine, Agreement No. F33/461-2009 with the Ministry for Education and Science of Ukraine. The research was also supported, in part, within a Ukrainian-Russian grant, Agreement No. Φ28/335-2009.

[1] L. D. Landau, Izv. Akad. Nauk SSSR Ser. Fiz. **17**, 51 (1953).
[2] Yu. M. Sinyukov, Nucl. Phys. A **566**, 589c (1994); in *Hot Hadronic Matter: Theory and Experiment*, edited by J. Letessier, H. H. Gutbrod, and J. Rafelski (Plenum, New York, 1995), p. 309.
[3] S. A. Bass and A. Dumitru, Phys. Rev. C **61**, 064909 (2000); D. Teaney, J. Lauret, and E. V. Shuryak, Phys. Rev. Lett. **86**, 4783 (2001); T. Hirano, U. Heinz, D. Kharzeev, R. Lacey, and Y. Nara, Phys. Lett. B **636**, 299 (2006); C. Nonaka and S. A. Bass, Phys. Rev. C **75**, 014902 (2007).
[4] W. Florkowski, W. Broniowski, M. Chojnacki, and A. Kisiel, Nucl. Phys. A **830**, 821c (2009).
[5] Yu. M. Sinyukov, S. V. Akkelin, and Y. Hama, Phys. Rev. Lett. **89**, 052301 (2002).
[6] S. V. Akkelin, Y. Hama, Iu. A. Karpenko, and Yu. M. Sinyukov, Phys. Rev. C **78**, 034906 (2008).
[7] Yu. M. Sinyukov, S. V. Akkelin, and Iu. A. Karpenko, Phys. At. Nucl. **71**, 1619 (2008).
[8] K. A. Bugaev, Phys. Rev. Lett. **90**, 252301 (2003).
[9] Yu. M. Sinyukov and Iu. A. Karpenko, Nonlinear Phenom. Complex Syst. **12**, 496 (2009).
[10] D. Teaney, Phys. Rev. C **68**, 034913 (2003).
[11] Z. Xu, L. Cheng, A. El, K. Gallmeister, and C. Greiner, J. Phys. G **36**, 064035 (2009).

[12] U. Heinz, J. Phys. G **31**, S717 (2005); P. Huovinen and P. V. Ruuskanen, Annu. Rev. Nucl. Part. Sci. **56**, 163 (2006); T. Hirano, Nucl. Phys. A **774**, 531 (2006).
[13] Yu. M. Sinyukov, Acta Phys. Pol. B **37**, 3343 (2006); M. Gyulassy, Iu. A. Karpenko, A. V. Nazarenko, and Yu. M. Sinyukov, Braz. J. Phys. **37**, 1031 (2007).
[14] T. Lappi and L. McLerran, Nucl. Phys. A **772**, 200 (2006).
[15] K. Werner, F. M. Liu, and T. Pierog, Phys. Rev. C **74**, 044902 (2006).
[16] J. Vredevoogd and S. Pratt, Phys. Rev. C **79**, 044915 (2009); S. Pratt, arXiv:0903.1469; W. Broniowski, W. Florkowski, M. Chojnacki, and A. Kisiel, Phys. Rev. C **80**, 034902 (2009).
[17] Yu. M. Sinyukov, Iu. A. Karpenko, and A. V. Nazarenko, J. Phys. G **35**, 104071 (2008).
[18] Yu. M. Sinyukov, A. V. Nazarenko, and Iu. A. Karpenko, Acta Phys. Pol. B **40**, 1109 (2009).
[19] P. F. Kolb, J. Sollfrank, and U. W. Heinz, Phys. Lett. B **459**, 667 (1999); U. W. Heinz and H. Song, J. Phys. G **35**, 104126 (2008).
[20] T. Lappi, Phys. Lett. B **643**, 11 (2006).
[21] A. Krasnitz and R. Venugopalan, Phys. Rev. Lett. **84**, 4309 (2000).
[22] A. Krasnitz, Y. Nara, and R. Venugopalan, Nucl. Phys. A **717**, 268 (2003).
[23] A. Krasnitz *et al.*, Nucl. Phys. A **727**, 427 (2003).
[24] A. Kovner, L. McLerran, and H. Weigert, Phys. Rev. D **52**, 6231 (1995).
[25] A. El, Z. Xu, and C. Greiner, Nucl. Phys. A **806**, 287 (2008).
[26] E. Wigner, Phys. Rev. **40**, 749 (1932).
[27] M. Hillery, R. F. O'Connell, M. O. Scully, and E. P. Wigner, Phys. Rep. **106**, 121 (1984); H.-W. Lee, *ibid.* **259**, 147 (1995); W. P. Schleich, *Quantum Optics in Phase Space* (Wiley-VCH, Weinheim, Germany, 2001).
[28] K. Werner, Phys. Rev. Lett. **98**, 152301 (2007).
[29] F. Becattini and J. Manninen, J. Phys. G **35**, 104013 (2008); J. Manninen and F. Becattini, Phys. Rev. C **78**, 054901 (2008).
[30] A. Andronic, P. Braun-Munzinger, and J. Stachel, Acta Phys. Pol. B **40**, 1005 (2009).
[31] M. Laine and Y. Schroder, Phys. Rev. D **73**, 085009 (2006).
[32] F. Karsch, PoS CPOD07:026, 2007.
[33] N. S. Amelin *et al.*, Phys. Rev. C **77**, 014903 (2008).
[34] Iu. A. Karpenko and Yu. M. Sinyukov, Phys. Lett. B **688**, 50 (2010).
[35] S. Mrowczynski, Ann. Phys. **169**, 48 (1986).
[36] M. Prakash, M. Prakash, R. Venugopalan, and G. Welke, Phys. Rep. **227**, 321 (1993).
[37] S. A. Bass *et al.*, Prog. Part. Nucl. Phys. **41**, 255 (1998).
[38] M. Holt, *Numerical Methods in Fluid Dynamics* (Springer, Berlin, 1977), Springer Series in Computer Physics.
[39] R. Courant, K. Friedrichs, and H. Lewy, IBM J. 215 (March 1967).
[40] V. Schneider *et al.*, J. Comput. Phys. **105**, 92 (1993).
[41] R. P. G. Andrade, F. Grassi, Y. Hama, T. Kodama, and W. L. Qian, Phys. Rev. Lett. **101**, 112301 (2008).
[42] Yu. M. Sinyukov, S. V. Akkelin, Iu. A. Karpenko, and Y. Hama, Acta Phys. Pol. B **40**, 1025 (2009).
[43] V. A. Averchenkov, A. N. Makhlin, and Yu. M. Sinyukov, Sov. J. Nucl. Phys. **46**, 905 (1987); A. N. Makhlin and Yu. M. Sinyukov, Z. Phys. C **39**, 69 (1988); Yu. M. Sinyukov, Nucl. Phys. A **498**, 151 (1989).
[44] J. Adams *et al.* (STAR Collaboration), Phys. Rev. Lett. **92**, 112301 (2004).
[45] J. Adams *et al.* (STAR Collaboration), Phys. Rev. C **71**, 044906 (2004).
[46] S. S. Adler *et al.* (PHENIX Collaboration), Phys. Rev. C **69**, 034909 (2004).
[47] S. S. Adler *et al.* (PHENIX Collaboration), Phys. Rev. Lett. **93**, 152302 (2004).
[48] S. Afanasiev *et al.* (PHENIX Collaboration), Phys. Rev. Lett. **103**, 142301 (2009).